Atmospheric Environment 385 (2026) 122349

Contents lists available at ScienceDirect

Atmospheric Environment

journal homepage: www.elsevier.com/locate/atmosenv

# Environmental controls of the soil sink of atmospheric hydrogen: a year-long study at a UK grassland using the aerodynamic gradient technique

Nicholas Cowan *, Mark Hanlon, Aurelia Bezanger, Chiara F. Di Marco, Carole Helfter, Neil J. Mullinger, Ruby Devlin, Toby Roberts, Sarah R. Leeson, Karen Yeung, Duncan Harvey, Eiko Nemitz, Julia Drewer

*UK Centre for Ecology and Hydrology Edinburgh, Bush Estate, Midlothian, EH26 0QB, UK*

## HIGHLIGHTS

- Continuous, year-long aerodynamic gradient (AG) measurement of $H_2$ fluxes.
- First field-scale micrometeorological flux measurements of $H_2$ in Europe.
- Soil moisture strongly controls $H_2$ flux in mineral grassland soils.
- AG method agrees well with flux chamber measurements of $H_2$ flux at site.

## ARTICLE INFO

*Keywords:*
$H_2$
Eddy covariance
Flux chamber
Micrometeorology
Soil moisture

## ABSTRACT

Atmospheric hydrogen ($H_2$) plays a significant role in tropospheric chemistry, yet substantial uncertainty remains surrounding the magnitude and controls of the global soil sink. We report the first year-long, continuous measurements of $H_2$ exchange using the aerodynamic gradient (AG) method at a temperate grassland. Despite the challenges associated with resolving small vertical gradients and the slow response time of GC instrumentation, the AG system produced a coherent record of ecosystem-scale $H_2$ uptake. Temporally aggregated data revealed that soil moisture was the dominant control of $H_2$ uptake at our site, with stronger uptake during warm, dry periods and minimal uptake when water-filled pore space was high (>50%). Soil temperature showed little independent effect once covariance with moisture was accounted for. The annual flux of two adjacent grassland fields was estimated to be −3.00 and −7.67 kg $H_2$ $ha^{-1}$ over the measurement period of September 2024 to September 2025 (mean deposition velocity ($V_{ds}$) of 0.20 and 0.51 mm $s^{-1}$). This study provides further evidence that the $H_2$ soil sink can be quantified accurately at the field scale using currently available micrometeorological methods but highlights the need for thorough temporal and spatial resolution measurements of soil parameters to better understand the drivers behind $H_2$ flux in soils.

## 1. Introduction

Molecular hydrogen ($H_2$) is the second most abundant reduced gas in the atmosphere after methane ($CH_4$), with a global mean mixing ratio of approximately 530 to 550 ppb (Paulot et al., 2024; Pétron et al., 2024) and an atmospheric lifetime between 1 and 3 years (Novelli et al., 1999). $H_2$ gas does not contribute to radiative forcing directly, as it is a diatomic molecule with no dipole moment (i.e., the molecules do not directly absorb infra-red radiation); however, competition with $CH_4$ and other trace gases (ozone and water vapour) for hydroxyl radicals (OH) influences the oxidative capacity of the atmosphere and affects the concentration and lifetime of greenhouse gases (GHGs) (Ocko and Hamburg, 2022; Warwick et al., 2023). Overall, the production of $H_2$ contributes indirectly to a net climate forcing, with a global warming potential (GWP) estimated between 3.3 and 11.6 over a 100-year time horizon (Derwent et al., 2020; Field and Derwent, 2021; Sand et al., 2023). With projected growth in $H_2$

* Corresponding author.
*E-mail address:* nicwan11@ceh.ac.uk (N. Cowan).

https://doi.org/10.1016/j.atmosenv.2026.122349
Received 22 June 2026; Received in revised form 1 September 2026; Accepted 6 September 2026
Available online 8 September 2026

production and use in energy systems as an energy carrier (e.g., the hydrogen economy) there is increasing concern that fugitive emissions of $H_2$ could offset some of the anticipated climate benefits of the reduction in the use of fossil fuels, particularly if activities lead to significant perturbations in the global $H_2$ budget (Ocko and Hamburg, 2022; Rezaei et al., 2025).

The global $H_2$ budget is dominated by two removal processes: oxidation in the atmosphere via reaction with OH radicals (10 to 30%) and uptake by soils (70 to 90%) (Ehhalt and Rohrer, 2009; Morfopoulos et al., 2012; Novelli et al., 1999; Rhee et al., 2006). The soil sink is mediated by hydrogen-oxidising bacteria that are ubiquitous in global soils and consume atmospheric $H_2$ (Baril and Constant, 2025; Greening et al., 2022; Hou et al., 2025). Microbial uptake of $H_2$ in soils (the soil sink) is widespread across ecosystems, but its magnitude and variability are strongly influenced by soil physical properties such as moisture, temperature, vegetation type, and land management (Cowan et al., 2025; Drewer et al., 2026; Meredith et al., 2014; Reji et al., 2025; Smith-Downey et al., 2008). Abiotic constraints can also impact the potential for $H_2$ uptake in soils, particularly the diffusion rate of $H_2$ into soils. Waterlogged or compacted soils with low diffusivity can minimise the exchange of $H_2$ between the atmosphere and active microbial layers in the soil, thus significantly reducing the potential for $H_2$ oxidation (Bertagni et al., 2021; Drewer et al., 2026; Smith-Downey et al., 2008).

Despite its importance, the soil sink remains one of the largest uncertainties in the global $H_2$ budget (Novelli et al., 1999; Ouyang et al., 2025; Rhee et al., 2006), and this uncertainty results in uncertainties in the other budget terms and its atmospheric lifetime overall. Observational coverage is limited, particularly for long-term, continuous flux measurements at the ecosystem scale. Most existing measurements of $H_2$ flux have been obtained using flux chambers at the plot or field scale (e.g. Baril et al., 2022; Cowan et al., 2025; Lallo et al., 2009; Smith-Downey et al., 2008). These approaches allow for concurrent soil and microbial measurements and can be deployed across diverse landscapes. However, chamber methods are inherently limited in their spatial representativeness, often sampling areas of less than 1 $m^2$ and are susceptible to artefacts such as pressure perturbations and alterations of diffusion rates between soil and atmosphere (Hudson and Ayoko, 2008; Xu et al., 2006). Temporal coverage is typically constrained to discrete campaigns or sporadic manual sampling, making it difficult to capture diurnal, seasonal, and interannual variability. Given that environmental conditions that alter the rate of microbial oxidation of $H_2$ in soils can vary over relatively short timescales (hours/days) due to changes in moisture (e.g., heavy rainfall) or temperature cycles, limited sampling schemes (using manual chambers) risk biasing flux estimates when extrapolated to annual budgets. Currently, there is a shortage of high temporal $H_2$ flux data which would allow for assessment of measurement methodologies, largely due to technical constraints of gas analysers and until recently, lack of interest in the topic.

For trace gases, micrometeorological flux measurement methods, such as the eddy covariance (EC) technique or the aerodynamic gradient (AG) method often offer an alternative method when estimating fluxes at the field scale. By measuring turbulent transport above the canopy, these methods integrate fluxes over relatively large homogeneous surfaces (100s of $m^2$) and capture semi-continuous time series of measurements, spanning weeks to years. For $H_2$, however, micrometeorological applications face significant challenges. The application of the EC methods requires fast measurement of gas concentrations ($\geq$10 Hz). Unlike commonly measured gases such as $CO_2$ or $H_2O$, there are no commercially available fast-response sensors for $H_2$ suitable for EC. Consequently, the AG approach, which can be implemented with slower-response sensors (such as gas chromatography) and then infers fluxes from vertical concentration gradients and turbulence measurements is one of the few micrometeorological methods capable of measuring $H_2$ flux between soil and atmosphere at the local level (e.g. Meredith et al., 2014). An alternative approach to infer fluxes averaged over a larger area from measurements is the application of inversion modelling (e.g. Simmonds et al., 2011). The AG method offers a feasible path to year-round $H_2$ flux measurements, but it brings its own methodological complexities. Gradient-based flux estimates rely on the accurate determination of small vertical concentration differences (often in the range of a few parts per billion) over measurement heights separated by only a few metres and therefore require precise measurement methods (Abdulwahab et al., 2025; Meredith et al., 2014).

Despite these challenges, long-term micrometeorological $H_2$ flux measurements are essential for improving process understanding and informing atmospheric models. Current global models parameterise the $H_2$ soil sink using biome-specific deposition velocities or empirical functions of soil temperature and moisture (Morfopoulos et al., 2012). These parameterisations are based on a limited set of field observations, often from short-term studies in North America, Europe or Japan, and may not capture the diversity of conditions in other regions. There is a particular lack of continuous, ecosystem-scale $H_2$ flux data from temperate grasslands, which cover large areas globally. Underestimation of sink strength, or mischaracterisation of its variability, can lead to biased projections of atmospheric $H_2$ burdens and associated impacts on the lifetime of GHGs such as $CH_4$ which ultimately determines the GWP of $H_2$ as a secondary GHG.

In this study, we aim to quantify the annual and seasonal variation in $H_2$ fluxes over a managed grassland at the long-term Easter Bush flux monitoring site in Scotland (UK) using the AG method and study their controls. We assess methodological performance between the AG and flux chamber methods (as reported in Cowan et al., 2025) as well as capability to predict $H_2$ fluxes based on environmental parameters. To our knowledge this work represents only the second time $H_2$ fluxes have been measured for more than a year using a micrometeorological technique, and the first time over grassland and in the UK. The dataset provides a unique opportunity to analyse the temporal dynamics of the exchange which would be missed with sporadic chamber measurements, and it constitutes an important reference point for both process-based understanding and the development of robust, regionally relevant parameterisations for atmospheric modelling.

## 2. Methods

### 2.1. Field site

Measurements were conducted at a long-term environmental monitoring site at Easter Bush Farm in Midlothian, central Scotland (55.8653° N, 3.206° W) from August 2024 until September 2025. The measurement location sits on the boundary between two adjacent fields, referred to as North and South (as in Cowan et al., 2020; Drewer et al., 2016). Both fields are intensively managed, improved grasslands used primarily for sheep grazing since 2001. Vegetation is dominated (>99%) by perennial ryegrass (*Lolium perenne*). The soil is classified as an imperfectly drained Eutric Cambisol with a silt loam texture. Management practices are typical for the region and include tractor-mounted broadcast applications of ammonium nitrate fertiliser, liming every 3–5 years to maintain soil pH between 5.5 and 6.0, and occasional ploughing and reseeding. Equipment was installed within a small, maintained, enclosed area with similar grass conditions as the fields, in which a permanently stationed, temperature-controlled cabin with access to mains power was located directly between the fields (Fig. 1). Nitrogen fertiliser as ammonium nitrate (Nitram®) was applied to the North and South fields on the 5th of April 2025 at a rate of 43.1 and 138 kg N $ha^{-1}$, respectively. The pH of the soil in the fields is approximately 5.5 and the sand/silt/clay ratio is 25/55/20 (as reported in Cowan et al., 2025).

### 2.2. Meteorological measurements

Meteorological measurement equipment was located in the enclosed area between the North and South fields (Fig. 1). Continuous measurements of soil temperature and soil volumetric water content (VWC) were made throughout the measurement period at 5, 10, 20 and 50 cm depth in the soil using buried CS655 water content reflectometers and CS109

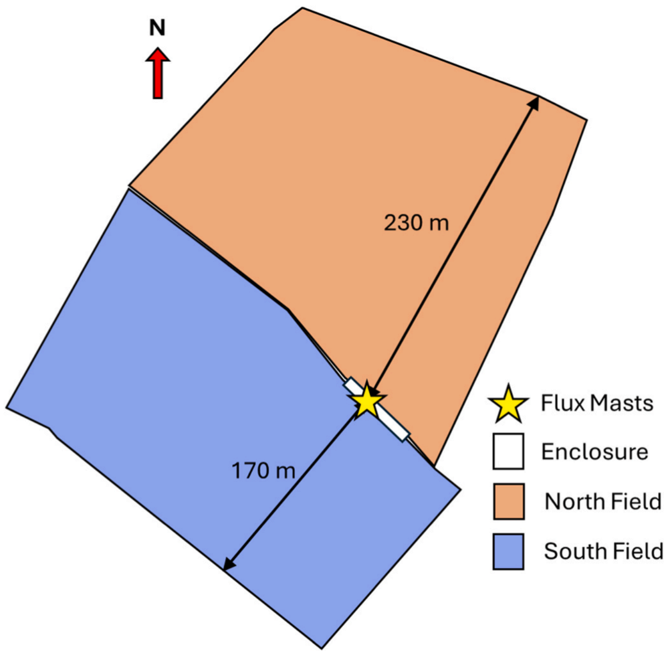


**Fig. 1.** $H_2$ flux and meteorological measurement equipment were positioned in an enclosed area between two grazed grassland fields at the Easter Bush permanent field site, Midlothian, Scotland, UK.

temperature probes (both Campbell Scientific, Utah, USA). Water filled pore space was calculated using a bulk density (BD) of 1.11 g cm$^{-3}$ and a particle density (PD) of 2.57 g cm$^{-3}$ (both measured in 2024 as reported in Cowan et al., 2025) as:

$$\%WFPS = \frac{VWC}{\left(1-\frac{BD}{PD}\right)} \times 100 \quad \text{Equation 1}$$

Air temperature and relative humidity were measured by a HMP60 Humidity and Temperature Probe (Vaisala, Vantaa, Finland) at a height of 1.85 m. A second mast was equipped with an ultra-sonic anemometer (R3-50, Gill, Lymington, UK) mounted at a height of 2.5 m to measure fluctuations in 3-D wind components at a frequency of 20 Hz. The prevailing wind direction at the site has historically been south-westerly (from the South Field) with occasional north-easterly winds (from the North field). During the flux measurement period, winds were typical, with predominant south-westerly winds from the direction of the South Field (76%) with a smaller coverage of the North Field (24%) (Fig. S1).

### 2.3. Aerodynamic gradient flux measurements of hydrogen

The AG method was used to measure gas fluxes of $H_2$, and also of $CO_2$ and $H_2O$ for comparison with collocated EC measurements for quality control. A mast with four inlet heights (0.55, 0.90, 1.70 and 3.05 m) was positioned within the enclosure between the North and South fields. A 16 m length of 1/4″ OD Dekabon tubing (Synflex 1300 Tube) was connected to each inlet and run along the protected conduit into the temperature-controlled cabin (Fig. S2). Each inlet line was connected to a separate 10 L stainless steel container housed within the cabin. Air was pumped continuously (VT4.4 rotary vane vacuum pump, Becker, Wuppertal, Germany) from the inlets to flush the steel containers at approximately 0.35 l min$^{-1}$, to provide more robust averages and reduce errors associated with sequential sampling. Solenoid valves (EVT307, SMC Corporation, Tokyo, Japan) were actuated to sequentially sample air from each of the four 10-L containers according to a set schedule into both the inlet of a gas chromatography (GC) instrument and a LI-7000 closed-path infrared gas analyser (LI-COR, Lincoln, Nebraska, USA).

Concentrations of $H_2$ were measured using an Agilent 8890 GC instrument (Agilent, Santa Clara, California, USA) fitted with a pulsed discharge helium ionisation detector (GC-PDHID). Each air sample took approximately 4 min to analyse, thus air from each of the four storage containers plus one sample from a gas cylinder with a known $H_2$ concentration of 534 ppb (the span standard) could be analysed on a fixed schedule every 30 min. Air from the different containers was simultaneously passed through the LI-7000, switching between containers every 3 min, and measuring concentrations of $CO_2$ and $H_2O$ at 1 Hz. Additional calibration standards of known $H_2$ concentrations (213, 448, 632 and 898 ppb, certified to ±5% BOC special gases, UK) were used to calibrate data from the GC instrument every 2-4 weeks of operation. Concentrations were also corrected via a span-gas ratio correction based on the ratio of difference between measured $H_2$ concentration against the span gas (every 30 min). Zero and span calibrations were carried out on the LI-7000 at least every 3 months, with the exception of spring 2025 where no calibration was performed.

Fluxes of gas species ($F_c$) calculated by the AG method require the mean measured vertical concentration gradient ($\partial\bar{c}/\partial z$) and an estimate of the turbulent diffusivity ($K_c$). Vertical concentration gradients of $H_2$ were estimated using a multi-level concentration–profile similar to that of Meredith et al. (2014). For each 30-min period, $H_2$ (1 sample per inlet height), $CO_2$ and $H_2O$ (using the mean of n > 300 samples per inlet height) concentrations were fitted to a vertical profile. Fluxes are based on Fick's law and the Monin–Obukhov similarity theory, with fluxes calculated as:

$$F_c = -K_c \frac{\partial\bar{c}}{\partial z} \quad \text{(Equation 2)}$$

Practical implementation of this equation can be simplified as the product of friction velocity ($u_*$) with the use of the von Kármán constant ($\kappa = 0.41$; Högström, 1996; Foken, 2006) such that:

$$F_c = -\frac{u_* \, \kappa\partial\bar{c}}{\partial\left[\ln(z-d) - \varphi_C\left(\frac{z-d}{L}\right)\right]} \quad \text{(Equation 3)}$$

where $d$ is the zero plane displacement, $L$ is the Monin–Obukhov length and $\varphi_C$ is the height-integrated stability correction function, which accounts for the distortion of atmospheric stability or instability in the inertial sublayer (Panofsky, 1963; Paulson, 1970). In neutral and stable conditions ($L > 0$ m), the stability correction of (Webb, 1970) is used (Equation (4)). For unstable conditions ($L < 0$ m), the stability correction of Paulson (1970) was used (Equation (5)).

$$\varphi_C = -5.2\,\frac{z-d}{L} \quad \text{(Equation 4)}$$

$$\varphi_C = 2\ln\left(\frac{1+x^2}{2}\right) \text{ where } x = \left(1-16\left(\frac{z-d}{L}\right)\right)^{0.25} \quad \text{(Equation 5)}$$

Wind speed at 1 m height was calculated as Equation (6). The deposition velocity ($V_d$) describes the rate at which a gas is transferred from the atmosphere to a surface (e.g. soil or vegetation), and it is typically expressed using a resistance-in-series model where $V_d$ is the inverse of the sum of the resistances (Seinfeld and Pandis, 2006). The aerodynamic resistance to scalar transport ($R_a$) was calculated using Equation (7), where ($\varphi_h$) and ($\varphi_m$) are the integrated stability correction functions for heat and momentum, respectively (Garland, 1977). The quasi-laminar boundary layer resistance ($R_b$) for hydrogen was calculated using Equation (8) where $\nu$ is the kinematic viscosity of air and $D_{H_2}$ is the molecular diffusivity of hydrogen in air ($7.0 \times 10^{-5}$ m$^2$ s$^{-1}$, engineeringtoolbox.com). The observed $V_d$ was calculated as the ratio of the measured hydrogen flux to the ambient hydrogen concentration (Equation (9)), where $F_{H_2}$ is the AG-derived hydrogen flux (nmol m$^{-2}$ s$^{-1}$) and $C_{H_2}$ is the corresponding atmospheric hydrogen concentration (nmol m$^{-3}$). Surface resistance ($R_c$) was calculated using Equation (10).

$$U_{1m} = \frac{u_*}{\kappa}\left[\ln\left(\frac{1\ \text{m}}{z_0}\right) - \varphi_m(1\ \text{m})\right] \quad \text{(Equation 6)}$$

$$R_a(1\ \text{m}) = \frac{U_{1m}}{{u_*}^2} - \frac{\varphi_h(1\ \text{m}) - \varphi_m(1\ \text{m})}{\kappa\, u_*} \quad \text{(Equation 7)}$$

$$R_b = \frac{1.45}{u_*}\left(\frac{z_0 u_*}{\nu}\right)^{0.24}\left(\frac{\nu}{D_{H_2}}\right)^{0.8} \quad \text{(Equation 8)}$$

$$V_d(1\ \text{m}) = -\frac{F_{H_2}}{C_{H_2}(1\ \text{m})} \quad \text{(Equation 9)}$$

$$R_c = \frac{1}{V_d(1\ \text{m})} - R_a(1\ \text{m}) - R_b \quad \text{(Equation 10)}$$

### 2.4. Supporting eddy covariance flux measurements

An eddy covariance (EC) mast was erected also in the enclosure between the North and South fields adjacent to the AG mast (2 m separation) (Fig. 1), to provide a reference measurement against which to assess the performance of the AG with fluxes of $CO_2$ measured by both systems. 3/8″ ID Dekabon tubing (Synflex 1300 Tube) was attached to the mast near the ultrasonic anemometer (northward, eastward and vertical separation from the centre of the sonic of 22, 5 and −5 cm, respectively). This 14 m inlet was run back along a protected conduit into a temperature-controlled cabin within the enclosure, where it was connected to a second LI-7000 closed-path gas analyser (LI-COR, Lincoln, Nebraska, USA). A rotary vane pump (VT4.4, Becker GmbH, Hull, UK) was used to draw air through the inlet and instrument with a flow rate of approximately 17 l $min^{-1}$. A 1 μm PTFE membrane air filter was fitted to the inlet of the instrument to prevent particulates from damaging the internal mirrors. Gas concentration data ($CO_2$ and $H_2O$) were recorded at 10 Hz. Data from the sonic anemometer and LI-7000 were logged synchronously using a custom-made program written in LabView™ (National Instruments, TX, USA). Zero and span calibrations were carried out at least every 3 months with the exception of Spring 2025 when no calibration was performed.

Fluxes of $CO_2$ were calculated over 30 min intervals using the EddyPro® software (Version 7.0.9, Li-COR, Lincoln, NE, U.S.A.), based on the covariance between gas concentration (χ) and vertical wind speed (w) (Equation (11)):

$$F_\chi = \overline{\chi' w'} \quad \text{Equation 11}$$

The time-lag between sonic anemometer and gas analyser were calculated using maximisation of covariance within a window of 0.5 to 1.1 s over the measurement period. In the flux calculation processing, we applied double coordinate rotation (vertical and crosswind), spike removal, block averaging and outlier removal of artefact measurements. The high and low frequency co-spectral attenuation of the system was corrected using the analytical method of Moncrieff et al. (1997). Corrections for density fluctuations in response to changes in temperature and humidity were applied on a half-hourly basis using the method of Ibrom et al. (2007).

### 2.5. Quality control and data filtering

Several stages of data filtering were applied to improve the quality of retained AG flux data. Initial filtering was based on wind conditions for which data was discarded when $u_* < 0.1$ m $s^{-1}$, $|L| < 2$ m, the variance in vertical wind speed > 1 m $s^{-1}$, or when wind was from the direction obscured either by the cabin (130 – 150°N) or by the fence line between the fields (305 - 315°N). As EC data was used to quality check AG fluxes, all data was discarded when $CO_2$ flux data was flagged for removal using the 0–1–2 quality flagging system by Mauder and Foken (2004). Where quality flags for sensible heat (*H*), momentum (*τ*) or $CO_2$ flux were 2, data was discarded from the analysis. Plausible limits on $CO_2$ flux at the site were deemed to be within −50 to 25 μmol $m^{-2}$ $s^{-1}$. Any EC flux data beyond these limits was also used to discard data. A further filtering of the $H_2$ data was applied based on the comparison of $CO_2$ flux measured using the AG and EC methods. Periods when measured $CO_2$ fluxes by both AG and EC methods differed by more than ± 10 μmol $m^{-2}$ $s^{-1}$ were taken as indicative that conditions for AGM calculations were not ideal, thus flux data was discarded from the analysis. After data filtering, approximately 37.3% of measured $H_2$ flux data remained.

### 2.6. Statistical analysis

All data analysis was carried out using the statistical software R (version 4.5.1) and R studio (R Core Team, 2025). Multiple regression models were fitted to $H_2$ flux using lm() function in the R package "*stats*" (R Core Team, 2025) using soil temperature and moisture measurements. A simplified general additive model (GAM) was used to generate a model fit to the flux data, accounting for nonlinear responses to environmental variables, implemented using the "*mgcv*" package for R (Wood, 2017). The GAM was fitted to flux data using measured soil temperature (10 and 50 cm depth), soil moisture (10 and 50 cm depth) and hour of day. Uncertainties in mean data are provided as 95% confidence intervals (CIs).

To aid in understanding the $H_2$ flux data collected during the campaign, a simplified uncertainty simulation was carried out to estimate the analytical uncertainty in fluxes calculated by the AG method based on the detection limit of the $H_2$ GC-PDHID instrument (i.e. to estimate measurement noise). Using randomly generated data of $u_*$ and *L* data constrained by the measured data for which flux data passed quality controls from the year-long experiment (Fig. S3a and S3b), the $H_2$ flux was simulated using $H_2$ concentrations based on random noise equivalent to the measurement uncertainty of the instrument ($H_2$ concentration of mean = 560 ppb, σ = ± 3 ppb). Using these constrained data distributions, a simulation of 10,000 repetitions of Equation (3) were carried out using friction velocity ($u_*$), Obukhov length (*L*) and $H_2$ concentration data to establish an approximation of the analytical noise of the method, essentially simulating the output of a range of zero flux conditions where only instrument noise and associated correction efforts are contributing to flux estimates. The results of this analysis were 95% quantiles of simulated $H_2$ flux of ± 21 nmol $m^{-2}$ $s^{-1}$ under stable conditions and ± 31 nmol $m^{-2}$ $s^{-1}$, under unstable conditions (Fig. S3c and d).

## 3. Results

### 3.1. Meteorological conditions

Seasonal variations in soil and air temperature during the measurement period were somewhat atypical of the site, with soil surface temperature ranging from a low of 2.2°C in mid-January, to a high of 19.1°C in mid-July (Fig. S4a). The average air temperature for the measurement period was 10.0 (sd ± 5.3)°C, somewhat above the running average of 8.4°C (20+ years of data), largely due to a warmer than usual winter during which no significant snow or freezing events occurred and a comparatively warm summer; however, previous years have seen similar mean temperatures, with 10.2°C recorded in 2023. Annual rainfall was significantly lower than normal. A total of 578 mm fell over the 410-day measurement period (1.1 years), less than half of the long-term annual average of 1040 mm (Fig. S4b). The severity of the lack of rainfall from March to June 2025 is rare in the region and local agricultural activities were affected by the dry conditions. As a result of this warm and dry period, soil moisture in the top 10 cm fell drastically during May 2025 from > 60% water-filled pore space (%WFPS) to less than 25% WFPS for several days (Fig. S4c). Observed %WFPS at the site varies by depth, with higher moisture content in the top 10 cm compared with surface (5 cm) and deeper measurements (>20 cm depth). This is the result of the compaction of the clay soil near the surface, caused by mechanical rolling of soil before the planting of grass seed. As such, there is a layer of compacted soil under the initial surface layer that retains water.

### 3.2. Flux measurements

A significant number of flux data points were excluded as a result of the quality control (QC) filters, largely due to limitations placed on $u_*$ and $L$ which resulted in the filtering out of approximately 30% of recorded data. A further 10% were excluded based on excessive deviation between EC and AG methods (for quality control purposes). Overall, 37.3% of recorded data was retained, the equivalent of 3,285 h of total measurement time.

Fluxes of $CO_2$ measured using the EC and AG methods were compared to assess the performance of the AG system. After applying quality-control filters to both datasets, the two methods showed good agreement, with a regression slope of 0.90 and an $R^2$ of 0.89 (Fig. S5). Measured fluxes from both methods follow regular diurnal patters and are relatively consistent throughout the year (Fig. 2), with deviation in June 2025 due to the combination of a grass cut causing a step change in fluxes and extended periods of missing data. There is a tendency for the AG method to slightly underestimate $CO_2$ fluxes during early morning hours (6 – 9 a.m.), which may be a result of the limitations of stability corrections during these periods. However, the methods generally agree and provide confidence that conditions are suitable for $H_2$ flux estimates without the need for further correction factors.

Ambient concentrations (mean of all inlet heights) of $H_2$ varied throughout the year, with a mean of all data of 568 ± 36 ppb and monthly means peaking at 624 ± 35 ppb in June 2025, with a minimum of 537 ± 20 ppb in September 2024 (Fig. S6a). Individual flux measurements (30-min intervals) of $H_2$ measured from the North and South fields ranged from −100 to 47 nmol $m^{-2}$ $s^{-1}$. The distribution of flux data was widely scattered, with similar patterns to analytical uncertainty simulation (less than 2.2% of measured data exceeded the upper limit of estimated statistical noise ± 31 nmol $m^{-2}$ $s^{-1}$) (Fig. 3a & b). Despite the relatively large noise in the 30-min flux data, there are still trends present in the flux data, with a statistically significant uptake when data is aggregated. The data distributions from the North and South fields suggest that uptake of $H_2$ in the North field is greater than that of the South field with means of −12.5 ± 8.7 and −4.8 ± 10.4 nmol $m^{-2}$ $s^{-1}$, respectively. Grouping data by month reveals a seasonal pattern in the data, showing that uptake of $H_2$ increased during the spring and summer, while remaining close to zero

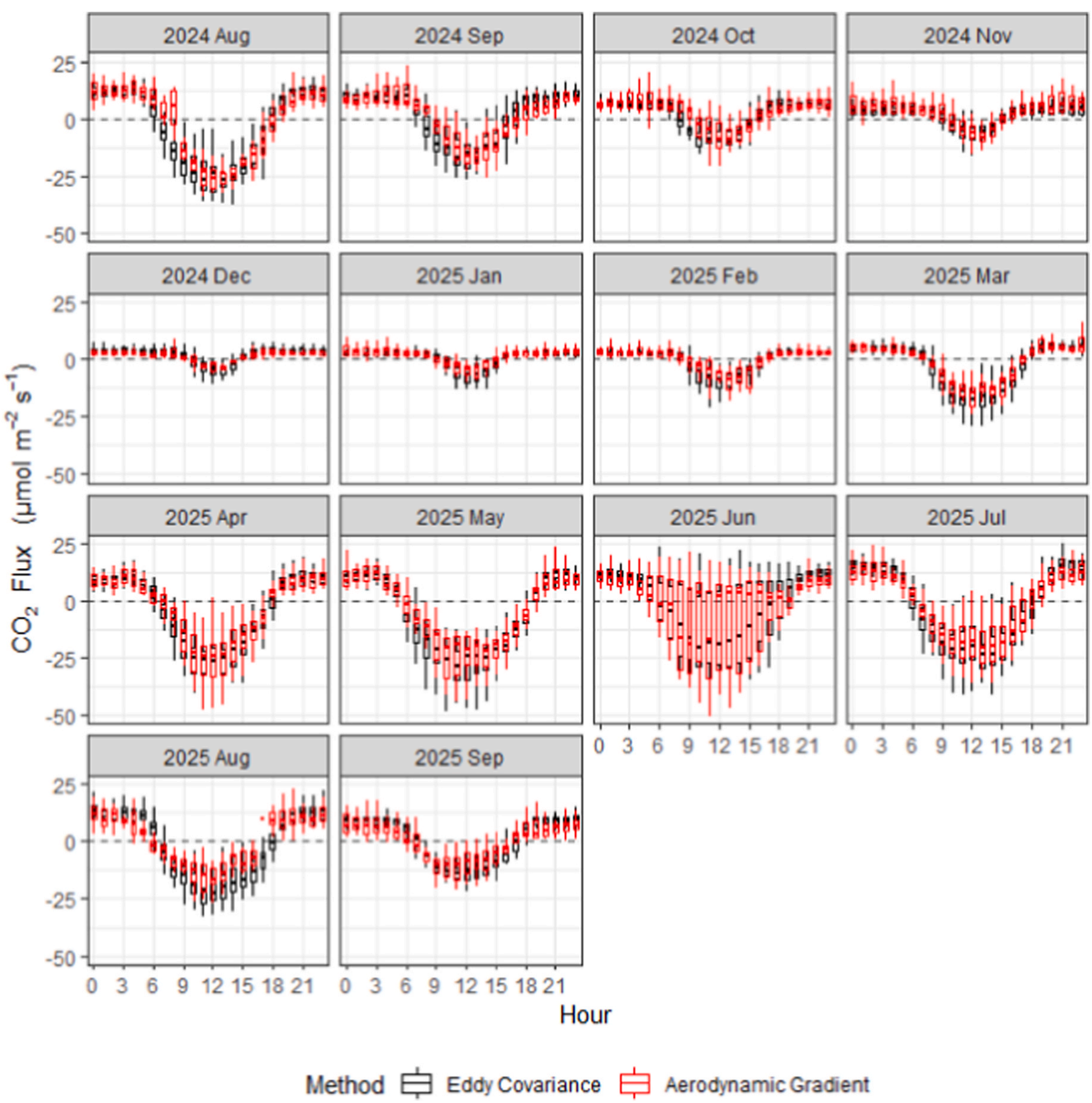


**Fig. 2.** Comparisons of hourly $CO_2$ flux measured using the EC and AG methods are made on a diurnal scale, splitting data by the month during which measurements were made. Boxplots, boxes and whiskers represent the median, 25th and 75th percentiles of data.

during winter (Fig. 3c). This pattern is also present in deposition velocity (Fig. S6b). The seasonal shift in flux magnitude is stronger for the North field, which consistently has greater monthly uptake of $H_2$ when compared to the South field.

### 3.3. Drivers of $H_2$ flux

The flux of $H_2$ at the site follows a strong seasonal trend. To explore the environmental controls on $H_2$ exchange, half-hourly fluxes were aggregated into daily means and compared with concurrent measurements of soil temperature and soil moisture (%WFPS) (Fig. 4). Although broad relationships between $H_2$ flux and these variables are evident (differing between fields) the data remain highly scattered, with individual regressions explaining little variance (maximum $R^2 \approx 0.3$). The large scatter in the flux data reflects both measurement uncertainty and intrinsic environmental variability, and consequently fitted relationships should be interpreted as describing broad tendencies rather than precise predictive functions. $H_2$ uptake generally increases under warm, dry soil conditions and declines toward zero during cold, wet periods. When the data are binned by temperature and moisture, soil moisture is a visibly strong driver of the $H_2$ flux, but the impact of soil temperature is less clear (Fig. S7). The apparent correlation with soil temperature largely reflects co-variation with moisture (e.g. warm, dry summers versus cold, wet winters), rather than a strong, independent temperature effect on microbial activity within the range observed at the site.

Grouping the data by month of measurement and using mean values reinforces the correlation between $H_2$ flux and environmental variables (Fig. 5). Monthly mean flux values clarify that fluxes tend toward zero and $H_2$ uptake at the site is lowest when the temperature at the field site is cold, and soil moisture is high. This is most visible during the winter when uptake in both fields is minimal ($<10$ nmol m$^{-2}$ s$^{-1}$). During the period of low rainfall in the spring and summer of 2025, the soil moisture content dropped significantly in the surface layers, and $H_2$ uptake increased drastically, with a mean flux in the North field in August 2025 of $-20.0 \pm 9.1$ nmol m$^{-2}$ s$^{-1}$ and -13.3 $\pm$ 11.2 nmol m$^{-2}$ s$^{-1}$ in the South field in September 2025 (Fig. 5a).

A weak but consistent diurnal pattern is present in the $H_2$ flux measurements for both the North and South fields (Fig. 6a). Although the magnitude of this pattern varies throughout the year, it persists across the measurement period (Fig. S9). Atmospheric $H_2$ concentrations also exhibit a weak diurnal cycle (Fig. 6c); however, the timing of the peak in $H_2$ concentration, which occurs later in the afternoon, is misaligned with the peaks in $H_2$ flux. This is reflected in the diurnal cycles of the deposition velocity ($V_d$), Fig. 6b), with both flux and $V_d$ peaking before midday. Deposition velocity provides a useful metric for interpreting surface–atmosphere exchange, as it represents the efficiency with which atmospheric $H_2$ is transferred to the surface and is widely used in chemical transport and chemistry–climate models to parameterise dry deposition processes.

Aerodynamic resistance ($R_a$ (1 m), Fig. 6e) showed only minor diurnal variability and remained small relative to other terms, while quasi-laminar resistance ($R_b$, Fig. 6f) exhibited a clear diurnal cycle driven by turbulence, with lower values during the daytime and higher values under stable night-time conditions. The surface resistance ($R_c$, Fig. 6g) dominated the total resistance and exhibited both strong diurnal variability and clear differences between fields. This indicates that $H_2$ deposition was primarily limited by surface processes rather than atmospheric transport, such that $V_d(1\,m) \approx 1/R_c$.

The differences observed between the North and South fields are primarily associated with variations in $R_c$, with consistently lower values in the North field indicating a stronger surface sink for $H_2$. These differences likely reflect contrasts in soil or vegetation properties between the fields, such as soil moisture, structure, or microbial activity, which influence the capacity for biological $H_2$ uptake.

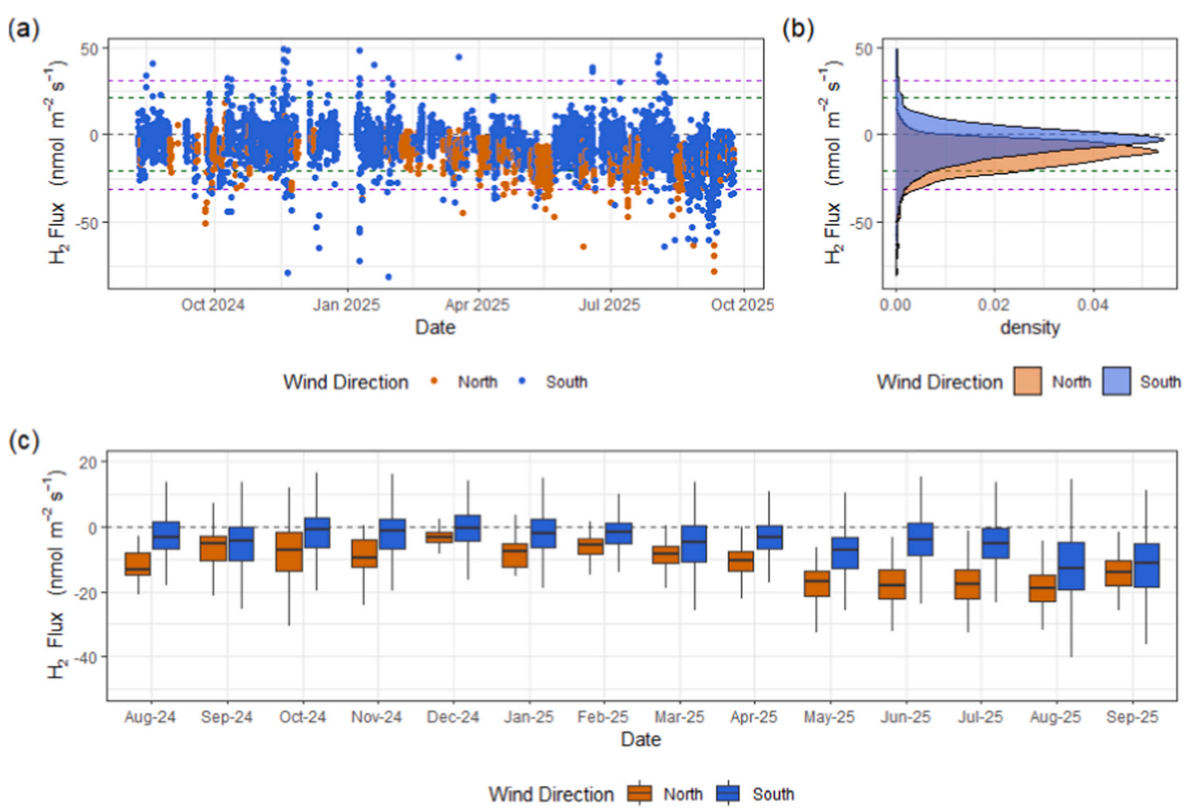


**Fig. 3.** (a) Individual flux measurements (30-min intervals) of $H_2$ measured from the North and South fields. (b) Density plot of $H_2$ flux data from the North and South fields. (c) Monthly binned $H_2$ flux data presented as boxplots, representing the median, 25th and 75th percentiles of data. Estimates of analytical uncertainty under stable (green dashed line) and unstable (purple dashed line) conditions and zero line (black dashed line) are included for comparison.

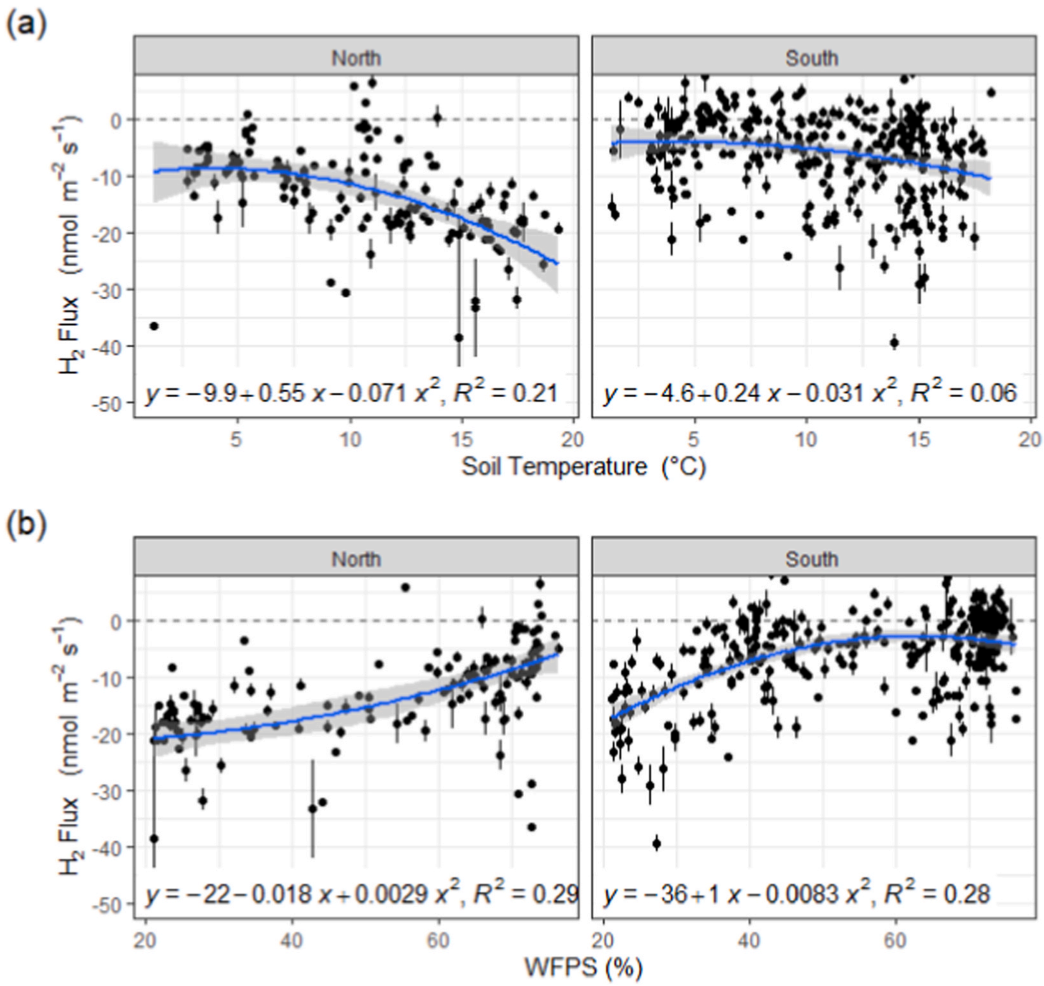


**Fig. 4.** Correlations between $H_2$ flux and (a) soil temperature and (b) water-filled pore space (WFPS) for the North and South fields separately (daily means). Soil temperature and WFPS were both measured at 10 cm depth. A second-order polynomial fit (blue) is included as a visual aid ($y = a_1x^2 + a_2x + c$). Error bars represent the 95% CIs in the daily mean where $n > 1$. Plots are trimmed from −50 to 5 nmol m$^{-2}$ s$^{-1}$. Shading represents the standard error in the fit. Presented as deposition velocity in Fig. S8.

Diurnal patterns in $R_c$ did not closely follow temperature or turbulence alone, implying additional control by soil microbial processes. The processes driving the observed diurnal variability in $H_2$ flux therefore remain unclear. The dominance of $R_c$ implies that diurnal variation in flux may reflect changes either in the rate at which $H_2$ diffuses into the soil (diffusion limitation) or in the rate at which soil microorganisms consume $H_2$ (microbial limitation). However, environmental variables typically associated with microbial activity, such as soil and air temperature, reach their maximum values after midday, whereas the peaks in $H_2$ flux and deposition velocity occur earlier in the day. Furthermore, no diurnal variation was observed in surface WFPS that would explain this trend in flux activity.

### 3.4. *$H_2$ flux gap-filling models*

As measurement data only covers 34% of the time between August 2024 and September 2025, gap-filling procedures are required to estimate a cumulative flux of $H_2$. Four different approaches were compared that consolidate predictions made using 30 min or daily mean data to provide estimates of mean monthly flux for each field separately: the first method was a straight block-averaging of the monthly fluxes available for each field (BLOCK). This effectively means gap-filling with the arithmetic monthly mean flux of the available flux data without consideration that the conditions during the gaps may not be the same as during the good data. Two approaches were then compared that make use of information of the local meteorological data (WFPS, soil temperature and $u_*$), The methods used were a non-linear regression (NLR) and a generalised additive model (GAM), both of which predicted $H_2$ flux on a 30-min basis. The final annual estimate was derived using the non-linear regression model predicted by historic flux chamber data (CH) using the parameters reported for measurements made at the site the previous year (using daily mean values for WFPS and soil temperature as reported in Cowan et al., 2025). The CH model was only developed for the South field from which measurements were made (non-linear regression parameters for NLR and CH methods provided in Table S1).

Direct comparison of the predictions from the different methods shows consistency across the methods (Fig. 7) and pairs well against the measured data ($R^2$ of modelled against block averaged data (BLOCK) ranging from 0.74 to 0.92) (Fig. S10). Based on the different methods, cumulative annual $H_2$ flux estimates from the fields from the 1st of September 2024 to 1st of September 2025 range from −2.61 to −3.58 kg $H_2$ ha$^{-1}$ for the South field, and −7.35 to −8.11 kg $H_2$ ha$^{-1}$ for the North field (Table 1). The aggregated monthly and yearly estimates agree relatively well. The blocked averages are sometimes larger and sometimes smaller than the monthly fluxes gap-filled with the NLR and GAM approaches suggesting that the $H_2$ flux during gaps is not overall systematically different to the flux during periods when measurements passed all quality criteria. The reasonable agreement with the CH method further suggests that the flux response was similar between the two measurement years and that the chamber measurements could parameterise the full response to meteorological controls

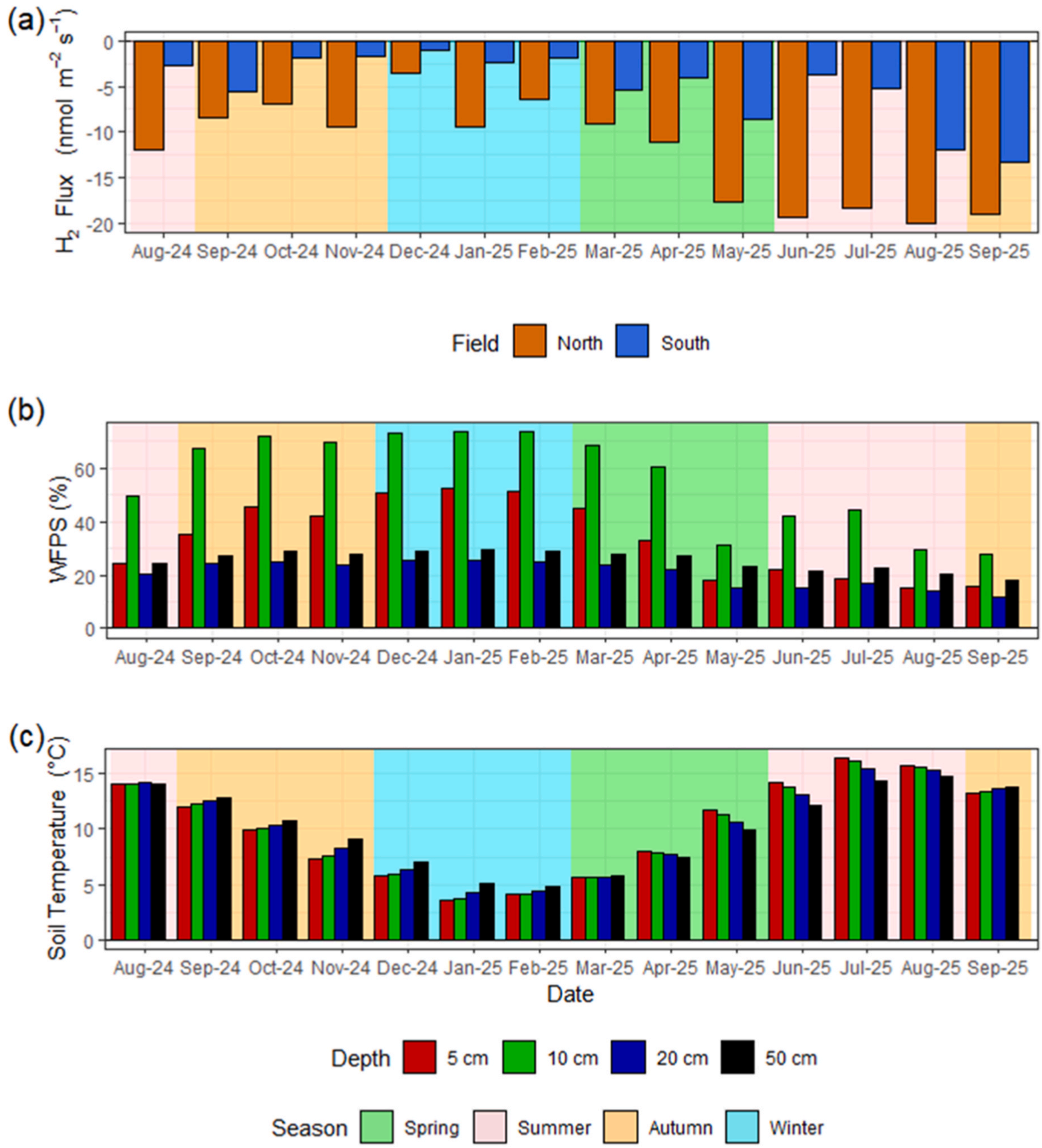


**Fig. 5.** Monthly mean data is presented for (a) $H_2$ flux, aggregated by wind direction, (b) water-filled pore space (WFPS) in the soil at four depths, and (c) soil temperature at four depths. A background colour scheme is used to highlight seasonal changes.

although they were only taken during daytime. By contrast, the gap-filling predictions vary in how well they represent diurnal activity. The CH method uses only daily averages of temperature and moisture variables and therefore cannot predict any diurnal activity in daily predictions. The NLR and GAM models do predict an element of diurnal activity in gap-filling procedures of 30-min data (Figs. S11 and S12). While the NLR method does not predict the diurnal pattern well, the flexible cubic spline method of the GAM model can incorporate the hour of day as an effective predicting parameter (fits a smooth curve to data by joining multiple third-degree polynomial segments at knots, while applying smoothing so the curve follows real trends without overfitting noise), thus the model predicts a strong diurnal pattern that matches measurement data reasonably well when sufficient data is present (Fig. S12).

## 4. Discussion

### 4.1. Methodological performance of the AG approach

Deployment of the aerodynamic gradient (AG) method is technically demanding and subject to several practical limitations. These constraints are especially pronounced for AG flux measurements of $H_2$ which is deposited very slowly ($V_d$(1 m) typically $< 0.5$ mm s$^{-1}$ at this site) at a comparably high atmospheric background concentration. This requires a very small relative gradient to be resolved by the analytical method. This is a fundamental limitation of gradient-based approaches for trace gases, where flux estimates rely on resolving concentration differences that are often close to analytical precision limits (Meredith et al., 2014; Moravek et al., 2014), constrained in this study by the precision of the gas chromatography analyser (σ = ±3 ppb). Because flux calculations depend on

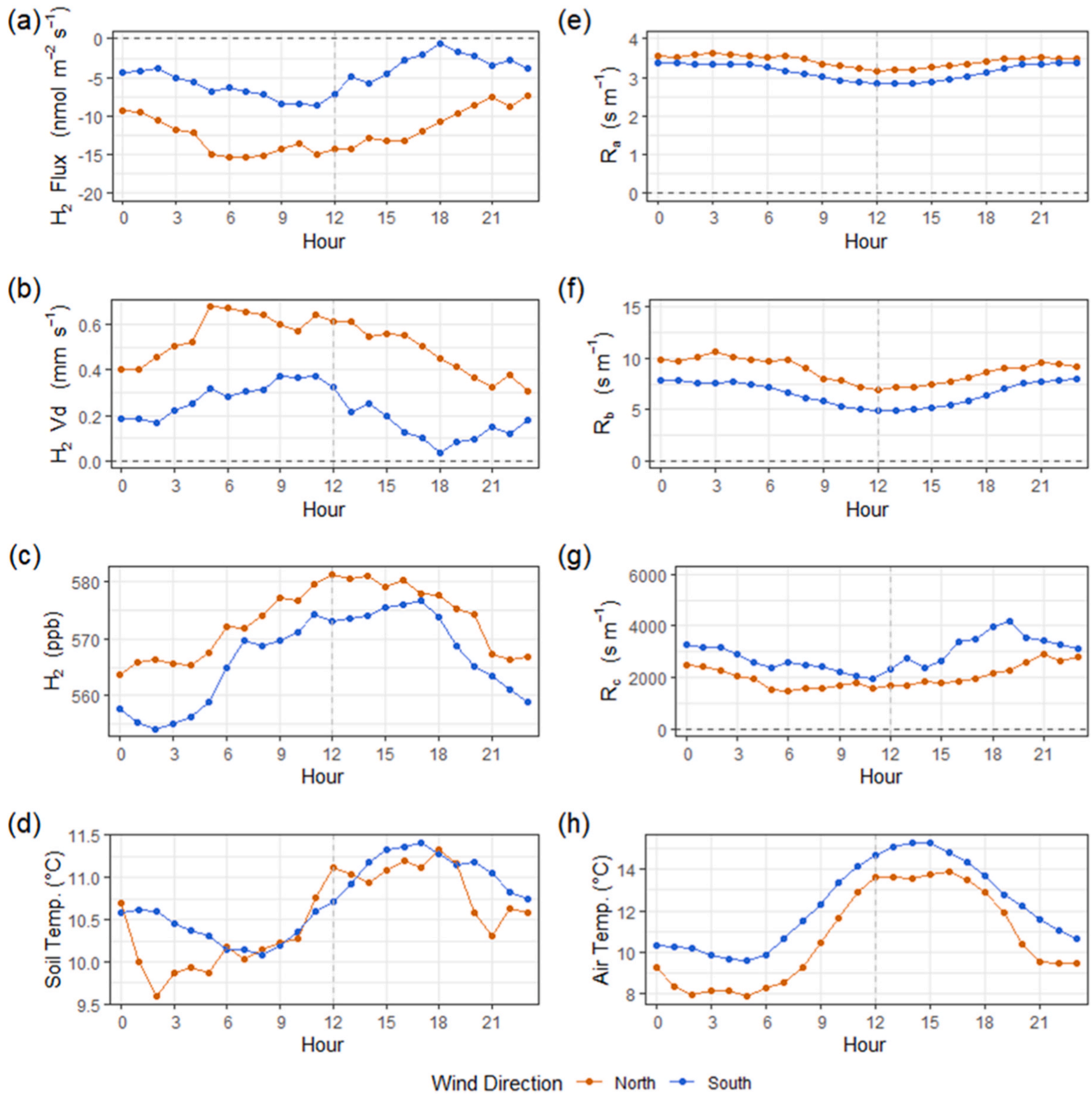


**Fig. 6.** Arithmetic mean values of data grouped by hour of day is presented to show typical diurnal trends in (a) $H_2$ flux, (b) $H_2$ deposition velocity (at 1 m), (c) $H_2$ atmospheric concentration (at 1m), (d) Soil temperature at 5 cm depth, (e) harmonic mean of aerodynamic resistance ($R_a$ at 1 m) of $H_2$ flux, (f) harmonic mean of quasi-laminar boundary resistance ($R_b$) of $H_2$ Flux, (g) harmonic mean of surface resistance ($R_c$) of $H_2$ Flux and (h) air temperature at 2.5 m height. Vertical dashed line included at midday (12:00) as a visual aid.

small differences between large background concentrations, random measurement error is rapidly amplified in the derived flux. In addition, the stability correction functions applied to account for atmospheric turbulence in the inertial sublayer rely on assumptions that are not always satisfied in the field, introducing additional sources of uncertainty. When these imperfect assumptions are combined with the inherently variable GC measurements and the exponential sensitivity of the derived vertical concentration gradient, the resulting flux estimates can carry substantial random errors. As the concentration gradient of $CO_2$ is much easier to resolve (higher concentrations, steeper concentration gradient and faster measurement method), comparisons of $CO_2$ flux derived by the AG method with those calculated using eddy covariance allow for a methodological check on the principles of the AG method. Comparison between $CO_2$ fluxes measured using both the AG and EC method agreed well, giving us confidence that micrometeorological conditions were adequate for the method to work after data filtering.

Our simplified simulation of analytical uncertainty demonstrates that the AG flux measurements are highly sensitive to noise in the gas concentration data. This sensitivity helps explain the wide scatter in individual flux estimates which is difficult to mitigate without faster and/or more precise instrumentation. Despite these substantial uncertainties at the half-hourly scale, aggregating the data into daily or monthly means markedly reduces random noise because of the large number of measurements available (nominally one every 30 min, though effective coverage was ~30% after QC), often deriving statistically significant fluxes and revealing seasonal and diurnal patterns. Importantly, the gap-filling regression models produced consistent flux predictions, including those derived from independent chamber measurements collected the previous year (with no temporal overlap) (Cowan et al., 2025).

### *4.2. Environmental controls on $H_2$ uptake*

The seasonal changes we observed in $H_2$ flux suggests that soil moisture exerts a stronger control on $H_2$ uptake than soil temperature at this site. During winter, when WFPS was consistently high throughout the soil profile, uptake rates in both fields remained low despite temperatures

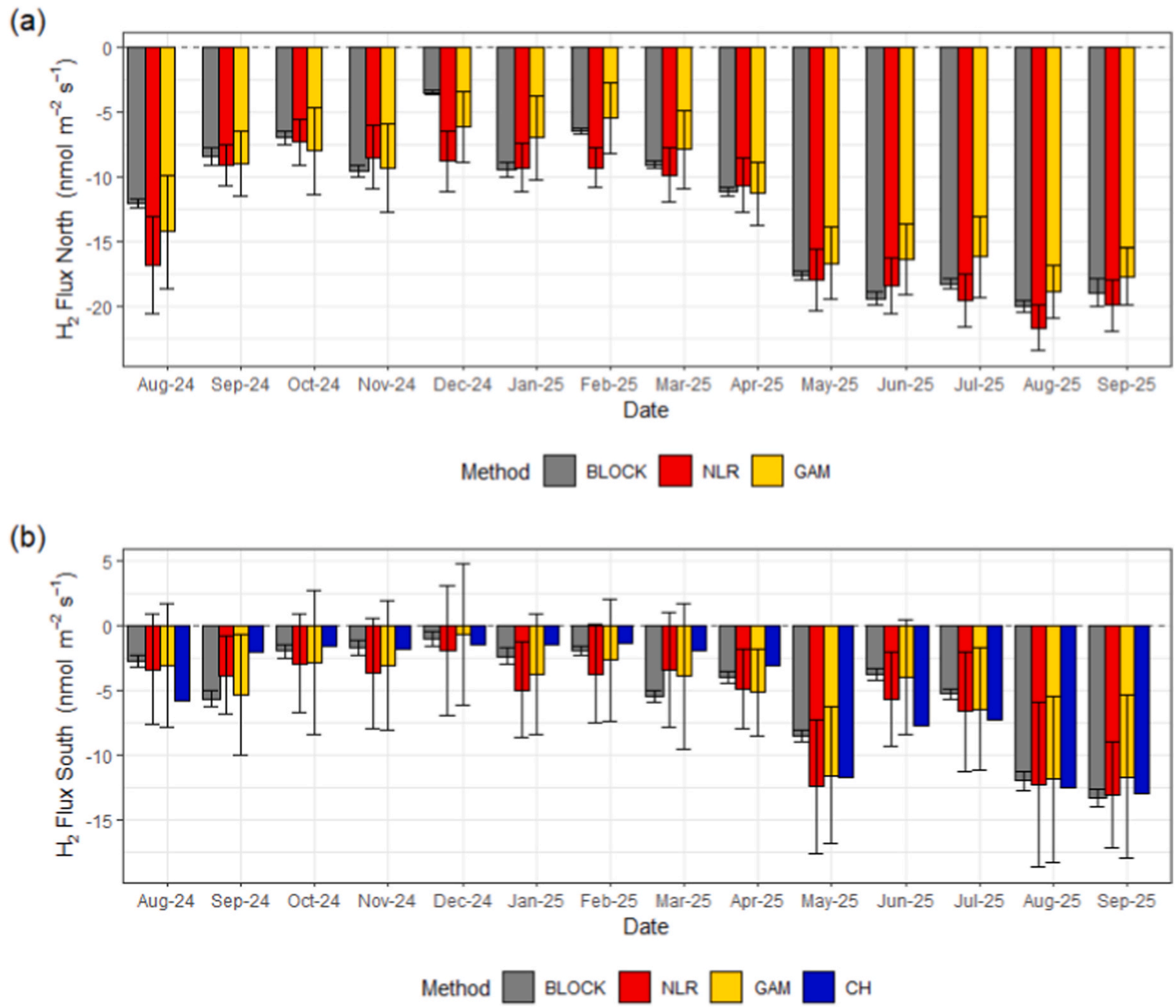


**Fig. 7.** Predictions of monthly mean $H_2$ flux from modelled outputs generated using block-averaged measurement data (BLOCK), non-linear regression (NLR), a generalised additive model (GAM) and the utilisation of the model predicted by historic flux chamber data (CH) measured from the South field. Error bars represent 95% CIs.

**Table 1**
Annual cumulative fluxes of $H_2$ predicted from the North and South fields by different parameterised models. The mean of all methods is also presented for each field.

| Field | Gap Filling Method | Cumulative $H_2$ Flux Annual Total (kg ha$^{-1}$) | Cumulative $H_2$ Flux 95% CI (kg ha$^{-1}$) |
|---|---|---|---|
| South | BLOCK | −2.89 | 0.58 |
| South | NLR | −3.58 | 0.39 |
| South | GAM | −2.61 | 0.36 |
| South | CH | −2.91 | 0.19 |
| **South** | **Mean** | **−3.00** | |
| North | BLOCK | −7.54 | 0.51 |
| North | NLR | −8.11 | 0.27 |
| North | GAM | −7.35 | 0.31 |
| **North** | **Mean** | **−7.67** | |

remaining within a range known to support microbial activity. In contrast, the pronounced increase in $H_2$ uptake during spring and summer coincided with a substantial reduction in soil moisture, particularly in the upper soil layers where diffusion of atmospheric $H_2$ into the soil occurs. This pattern is consistent with a diffusion-limited system in which increasing soil water content restricts the movement of atmospheric $H_2$ through air-filled pore space and reduces accessibility of $H_2$ to hydrogen-oxidising microorganisms. Soil temperature may still influence microbial activity, but within the relatively small range of temperatures observed at the site during dry conditions, its effect appears secondary to the strong control exerted by soil moisture.

The strong inter-annual agreement in flux magnitude measured and predicted by the AG and chamber method is encouraging and increases confidence that both methods captured $H_2$ fluxes reliably at this site. The only other AG $H_2$ flux dataset published to date is that of Meredith et al. (2014) where flux data was also aggregated to account for high random uncertainty. Although predictive models used for gap-filling in this study converged on similar conclusions, each carries specific strengths and limitations that should be considered. For any approach to yield reliable predictive models, flux measurements must span the full range of environmental conditions that will later require gap-filling (e.g. covering wet and dry periods, hot and cold seasons, and any other relevant extremes). For the AG method, achieving this coverage is relatively straightforward provided the system operates reliably for most of the year and wind conditions yield sufficient data after QC filtering. In contrast, flux-chamber campaigns require substantially more effort to capture rarer environmental conditions, often necessitating measurements during unfavourable weather. Chamber measurements are less affected by uncertainties in micrometeorological corrections but are instead vulnerable to large spatial and temporal heterogeneity that can be difficult to characterise, specifically that of diurnal activity which may bias flux estimates if not accounted for.

### 4.3. Diurnal and spatial variability in $H_2$ fluxes

Due to the lack of availability of high-resolution measurement methods and the relatively few studies on $H_2$ flux in literature, there is limited understanding of the potential diurnal behaviour of $H_2$ flux in soils, though those that have investigated typically do find diurnal patterns in measurements. Constant et al. (2008) and Yonemura et al. (2000) both report a similar diurnal pattern in $H_2$ uptake in soils, with peaks in uptake occurring in the middle of the day. Yonemura et al. (2000) attribute this to the variation in water moisture in the field caused by evaporation, but report that this relationship was constrained to an extent by the leaf layer above the soil. Constant et al. (2008) note that the diurnal pattern observed in their measurements only occurs between 10 and 20°C and do not attribute a specific driver to its occurrence. A diurnal pattern in $H_2$ flux is also observed by Meredith et al. (2014) with the highest soil uptake of $H_2$ occurring during midday in warmer summer months.

The underlying mechanism of the diurnal behaviour of $H_2$ uptake at the site in this study has proven difficult to determine based on the measurement data we have. The pattern does not appear linked to changes in ambient $H_2$ concentration. Ambient concentrations of $H_2$ varied diurnally and throughout the year, following an annual cycle similar to that reported in Forster et al. (2012) with a peak in late spring to early summer and a trough late summer into winter. The lack of correlation with changing ambient $H_2$ concentrations and the diurnal variability in $R_c$ ($V_d$) suggest that, at least at our site, limitations imposed by soil conditions are dictating variability in $H_2$ uptake. Unlike patterns observed in other studies, where $H_2$ peaks at midday, an increasing uptake of $H_2$ is observed in the early hours of the morning at our site, with peaks in soil uptake occurring several hours before maximum soil temperatures are reached. It is unclear if this suggests that the pattern is driven by something other than microbial activity and possibly a real signal influenced by an additional artefact.

The reason for the large difference in $H_2$ uptake observed between the fields is uncertain. Both fields are managed similarly (with occasional tillage/silage management rotation) and are similar in terms of soil structure, pH, carbon content and stocking density (Cowan et al., 2020; Drewer et al., 2016). Differences in air temperature and $H_2$ concentrations are observable in data collected from the two predominant wind directions at the site (North-Easterly and South-Westerly); however, these variables do not explain consistent differences in measured $H_2$ flux or deposition velocities across the two fields. We observe statistically significant correlation between $H_2$ flux and soil moisture measured at the site, consistent with previous work showing that soil H2 uptake is often diffusion-limited, with moisture exerting a dominant control through its effect on gas diffusivity within the soil profile (Smith-Downey et al., 2008). However, the singular measurement location of soil parameters placed at the foot of the tower (between both fields) does not describe spatial differences. Despite adjacent location, similar soils and long-term management, $H_2$ uptake in the fields varied by more than a factor of 2. Given that micrometeorological flux measurements integrate over a spatially variable footprint that shifts with atmospheric conditions (Kljun et al., 2015), differences in soil moisture or drainage within the contributing area may strongly influence observed fluxes. The South field sits at the bottom of a slope and under field drainage was damaged several years ago at the East side of the field during digging works. In contrast, the North field is situated on slightly higher ground and does not exhibit the same tendency toward localised waterlogging. The area near the enclosure can become boggy at times in the South field, more so than the North side, indicating differences in WFPS that will not be detected by a single measurement position. Given the strong sensitivity of $H_2$ uptake to soil moisture observed in both this study and previous work, relatively small differences in drainage status across the flux footprint could produce substantial differences in $H_2$ uptake, even between adjacent fields. The lack of spatial measurements and the accurate assessment of soil conditions within the flux footprint at any given time is a limitation when assessing flux measured via micrometeorological methods. Where flux is spatially variable due to spatially heterogenous factors such as soil moisture, predictive models are limited in accuracy. As variability in $H_2$ flux at the local scale is strongly tied to the moisture content of the soil (which controls diffusion), we would recommend further efforts to pair flux footprint with more detailed soil moisture measurements in future studies.

### 4.4. Implications for future $H_2$ flux measurements and global budgets

The mean fluxes reported from the fields, −12.5 and −4.8 nmol m$^{-2}$ s$^{-1}$ for the North and South fields, respectively, compare well with the available literature values (Table 2). Studies carried out in urban areas such as Lallo et al. (2009) and Hammer and Levin (2009) report mean $H_2$ fluxes in the region of −6.4 to −19 nmol m$^{-2}$ s$^{-1}$, and mean fluxes from arable fields made by Baril et al. (2022) and Nagai et al. (2024) range from −5 to −10 nmol m$^{-2}$ s$^{-1}$. In our study, annual uptake of $H_2$ in the North and South fields was estimated at approximately 7.9 and 3.5 kg ha$^{-1}$, respectively, for the measurement period between 1st September 2024 to 1st September 2025. Although $H_2$ fluxes clearly vary with climate, soil characteristics, vegetation type and microbial composition, upscaling of our fluxes to the Earth's terrestrial surface area can provide a sense-check of the results: the two field estimates scale to global totals of 44 and 114 Mt yr$^{-1}$, which would be broadly in the range of magnitude of the current estimate of 54 (47-61) Mt yr$^{-1}$ (Sand et al., 2023).

**Table 2**
A summary of $H_2$ flux and deposition velocity ($V_d$) measurements reported in literature, compared with measured values in this study. Mean values and reported uncertainties. Where only flux or $V_d$ is reported, missing values are estimated using an ambient $H_2$ concentration of 500 ppb.

| Study | Soil Type | Country | Mean $H_2$ Flux (nmol m$^{-2}$ s$^{-1}$) | Mean $V_d$ (mm s$^{-1}$) |
|---|---|---|---|---|
| This Study | Grass (South) | UK (SCO) | −4.8 ± 10.4 | 0.20 ± 0.35 |
| | Grass (North) | UK (SCO) | −12.5 ± 8.7 | 0.51 ± 0.35 |
| Yonemura et al. (2000) | Arable | JAP | 0 to −19.8 | 0 to 0.9 |
| | Forest | (TYO) | −11 to −17.6 | 0.5 to 0.8 |
| Rahn et al. (2002) | Forest | USA (AK) | −2.0 to −12.0 | 0.91 to 0.54 |
| Lallo et al. (2009) | Urban/ Forest | FIN (KH) | −5.1 to −12.1 | 0.23 to 0.55 |
| Smith-Downey et al. (2008) | Forest | USA (CA) | −7.9 ± 4.2 | 0.63 ± 0.29 |
| | Desert | USA (CA) | −7.6 ± 5.3 | 0.51 ± 0.36 |
| | Marsh | USA (CA) | −7.5 ± 3.4 | 0.35 ± 0.13 |
| Lallo et al. (2009) | Urban Park | FIN (Hesa) | −10.0 ± 2.5 | 0.20 ± 0.05 |
| | Urban Park | FIN (Hesa) | −19.0 ± 3.5 | 0.38 ± 0.07 |
| Hammer and Levin (2009) | Urban/ Agriculture | GER (BW) | −6.4 ± 1.6 | 0.3 ± 0.07 |
| Yver et al. (2009) | Urban | FRA (IDF) | −5.28 ± 2.86 | 0.24 ± 0.13 |
| Simmonds et al. (2011) | Peatland | IRE (GAL) | −26.5 (−9.0 to −64.5) | 0.53 (0.18 – 1.29) |
| Forster et al. (2012) | Coastal | UK (ENG) | −9.7 to −2.9 | 0.13 to 0.44 |
| Bartyzel et al. (2013) | Grass | PL (KOM) | −6.4 ± 3.3 | 0.03 ± 0.02 |
| Meredith et al. (2016) | Woodland | USA (MA) | −3.2 ± 1.6 | 0.03 to 0.43 |
| Baril et al. (2022) | Arable | CAN (QC) | −5.9 ± 4.3 | 0.12 ± 0.09 |
| Buzzard et al. (2022) | Desert (Monsoon) | USA (AZ) | −1.5 to −3.5 | 0.3 to 0.07 |
| Nagai et al. (2024) | Arable | JAP (JP02) | −5 to −10 | 0.1 to 0.2 |
| Cowan et al. (2025) | Grass | UK (SCO) | −2.6 ± 0.4 | 0.12 ± 0.02 |
| | Woodland | UK (SCO) | −18.2 ± 1.0 | 0.88 ± 0.05 |

Looking ahead, improving flux-measurement accuracy for $H_2$ will likely depend on advances in instrumentation. If fast-response analysers capable of high-precision $H_2$ measurements were used instead of GC systems, analytical uncertainty could be reduced dramatically. For example, we predict using an instrument with a precision of ~5 ppb at 0.2 Hz resolution (e.g. Aerodyne's TILDAS $H_2$ Monitor, Momeni et al., 2025) would reduce the simulated uncertainty in our study from ± 31 nmol $m^{-2}$ $s^{-1}$ to ± 5 nmol $m^{-2}$ $s^{-1}$ under stable conditions. Reducing the cost and technical demand of such measurements in future would also increase the uptake of these techniques by researchers, allowing for the collection of more long-term measurement data (multiple years) and the capture of extreme weather events. Such improvements would represent a major step forward for micrometeorological approaches such as the AG method.

## 5. Conclusions

This study provides only the second continuous, year-long aerodynamic gradient (AG) measurement of $H_2$ fluxes, and the first over a temperate grassland. Despite the inherent challenges of the AG technique, the method successfully captured the dominant patterns in soil $H_2$ uptake at the site. Measurements demonstrated that soil moisture was the primary control of microbial uptake of $H_2$, with periods of high soil water content sharply suppressing uptake, while warm, dry conditions enhanced it, consistent with diffusion-limited microbial consumption of atmospheric $H_2$. The successful year-long deployment demonstrates that continuous ecosystem-scale monitoring of $H_2$ is both feasible and informative, highlighting the value of micrometeorological approaches for improving our understanding of the soil $H_2$ sink.

## CRediT authorship contribution statement

**Nicholas Cowan:** Writing – original draft, Visualization, Validation, Methodology, Investigation, Formal analysis, Data curation. **Mark Hanlon:** Writing – review & editing, Methodology, Investigation, Data curation. **Aurelia Bezanger:** Methodology, Investigation, Data curation. **Chiara F. Di Marco:** Writing – original draft, Validation, Methodology, Formal analysis, Data curation. **Carole Helfter:** Writing – review & editing, Software, Methodology, Investigation, Data curation. **Neil J. Mullinger:** Writing – review & editing, Methodology, Investigation, Data curation. **Ruby Devlin:** Writing – review & editing, Methodology, Investigation, Data curation. **Toby Roberts:** Methodology, Investigation, Data curation. **Sarah R. Leeson:** Writing – review & editing, Methodology, Investigation, Formal analysis, Data curation. **Karen Yeung:** Writing – review & editing, Software, Methodology, Investigation, Data curation. **Duncan Harvey:** Writing – review & editing, Methodology, Investigation. **Eiko Nemitz:** Writing – original draft, Validation, Supervision, Resources, Methodology, Investigation, Funding acquisition, Conceptualization. **Julia Drewer:** Writing – original draft, Validation, Supervision, Project administration, Investigation, Conceptualization.

## Declaration of competing interest

The authors declare that they have no known competing financial interests or personal relationships that could have appeared to influence the work reported in this paper.

## Acknowledgments

This research has been supported by the Natural Environment Research Council grants The Enigma of the Soil Hydrogen Sink Variability [ELGAR] (NE/X013456/1), and the National Capability for UK Challenges Programme (NE/Y006208/1).

## Appendix A. Supplementary data

Supplementary data to this article can be found online at https://doi.org/10.1016/j.atmosenv.2026.122349.

## Data availability

https://doi.org/10.5285/077FECC1-6244-4FD7-9D41-6F98763F5F14.

## References

Abdulwahab, M.O., Flechard, C., Fauvel, Y., Häni, C., Jacotot, A., Graux, A.-I., Edouard, N., Buysse, P., Viaud, V., Neftel, A., 2025. Aerodynamic flux–gradient measurements of ammonia over four spring seasons in grazed grassland: environmental drivers, methodological challenges and uncertainties. Biogeosciences 22, 6669–6693. https://doi.org/10.5194/bg-22-6669-2025.

Baril, X., Constant, P., 2025. Life history strategies to study the succession of H2-oxidizing bacteria and their ecological role along $H_2$ concentration gradients in upland soils. Lett. Appl. Microbiol. 78. https://doi.org/10.1093/lambio/ovaf061.

Baril, X., Durand, A.-A., Srei, N., Lamothe, S., Provost, C., Martineau, C., Dunfield, K., Constant, P., 2022. The biological sink of atmospheric $H_2$ is more sensitive to spatial variation of microbial diversity than $N_2O$ and $CO_2$ emissions in a winter cover crop field trial. Sci. Total Environ. 821, 153420. https://doi.org/10.1016/j.scitotenv.2022.153420.

Bartyzel, J., Necki, J.M., Zieba, D., Rozanski, K., Gasiorek, M., 2013. Uptake of atmospheric hydrogen by soils: a case study from southern Poland. Eur. J. Soil Sci. 64, 597–609. https://doi.org/10.1111/ejss.12066.

Bertagni, M.B., Paulot, F., Porporato, A., 2021. Moisture fluctuations modulate abiotic and biotic limitations of $H_2$ soil uptake. Glob. Biogeochem. Cycles 35. https://doi.org/10.1029/2021gb006987.

Buzzard, V., Thorne, D., Gil-Loaiza, J., Cueva, A., Meredith, L.K., 2022. Sensitivity of soil hydrogen uptake to natural and managed moisture dynamics in a semiarid urban ecosystem. PeerJ 10, e12966. https://doi.org/10.7717/peerj.12966.

Constant, P., Poissant, L., Villemur, R., 2008. Annual hydrogen, carbon monoxide and carbon dioxide concentrations and surface to air exchanges in a rural area (Québec, Canada). Atmos. Environ. 42, 5090–5100. https://doi.org/10.1016/j.atmosenv.2008.02.021.

Cowan, N., Levy, P., Maire, J., Coyle, M., Leeson, S.R., Famulari, D., Carozzi, M., Nemitz, E., Skiba, U., 2020. An evaluation of four years of nitrous oxide fluxes after application of ammonium nitrate and urea fertilisers measured using the eddy covariance method. Agric. For. Meteorol. 280, 107812. https://doi.org/10.1016/j.agrformet.2019.107812.

Cowan, N., Roberts, T., Hanlon, M., Bezanger, A., Toteva, G., Tweedie, A., Yeung, K., Deshpande, A., Levy, P., Skiba, U., Nemitz, E., Drewer, J., 2025. Quantifying the soil sink of atmospheric hydrogen: a full year of field measurements from grassland and forest soils in the UK. Biogeosciences 22, 3449–3461. https://doi.org/10.5194/bg-22-3449-2025.

Derwent, R.G., Stevenson, D.S., Utembe, S.R., Jenkin, M.E., Khan, A.H., Shallcross, D.E., 2020. Global modelling studies of hydrogen and its isotopomers using STOCHEM-CRI: likely radiative forcing consequences of a future hydrogen economy. Int. J. Hydrogen Energy 45, 9211–9221. https://doi.org/10.1016/j.ijhydene.2020.01.125.

Drewer, J., Anderson, M., Levy, P.E., Scholtes, B., Helfter, C., Parker, J., Rees, R.M., Skiba, U.M., 2016. The impact of ploughing intensively managed temperate grasslands on $N_2O$, $CH_4$ and $CO_2$ fluxes. Plant Soil 411, 193–208. https://doi.org/10.1007/s11104-016-3023-x.

Drewer, J., Cowan, N.J., Hanlon, M., Roberts, T., Karbin, S., Devlin, R., Nalavade, R., Nemitz, E., Tweedie, A., Bezanger, A., 2026. Characterizing environmental drivers of the soil hydrogen sink through controlled laboratory experiments. https://doi.org/10.2139/ssrn.6222017.

Ehhalt, D.H., Rohrer, F., 2009. The tropospheric cycle of $H_2$: a critical review. Tellus B 61, 500. https://doi.org/10.1111/j.1600-0889.2009.00416.x.

Field, R.A., Derwent, R.G., 2021. Global warming consequences of replacing natural gas with hydrogen in the domestic energy sectors of future low-carbon economies in the United Kingdom and the United States of America. Int. J. Hydrogen Energy 46, 30190–30203. https://doi.org/10.1016/j.ijhydene.2021.06.120.

Foken, T., 2006. 50 years of the Monin–Obukhov similarity theory. Boundary-Layer Meteorol. 119, 431–447. https://doi.org/10.1007/s10546-006-9048-6.

Forster, G.l., Sturges, W.T., Fleming, Z.l., Bandy, B.J., Emeis, S., 2012. A year of $H_2$ measurements at Weybourne Atmospheric Observatory, UK. Tellus B 64, 17771. https://doi.org/10.3402/tellusb.v64i0.17771.

Garland, J.A., 1977. The dry deposition of sulphur dioxide to land and water surfaces. Proc. Roy. Soc. London. A. Math. Phys. Sci. 354, 245–268. https://doi.org/10.1098/rspa.1977.0066.

Greening, C., Islam, Z.F., Bay, S.K., 2022. Hydrogen is a major lifeline for aerobic bacteria. Trends Microbiol. 30, 330–337. https://doi.org/10.1016/j.tim.2021.08.004.

Hammer, S., Levin, I., 2009. Seasonal variation of the molecular hydrogen uptake by soils inferred from continuous atmospheric observations in Heidelberg, southwest Germany. Tellus B 61, 556. https://doi.org/10.1111/j.1600-0889.2009.00417.x.

Högström, U., 1996. Review of some basic characteristics of the atmospheric surface layer. Boundary-Layer Meteorol. 78, 215–246. https://doi.org/10.1007/bf00120937.

Hou, L., Whalen, J.K., Constant, P., 2025. Ecological traits of high-affinity hydrogen-oxidizing soil bacteria involved in the hydrogen cycle. Soil Biol. Biochem. 207, 109831. https://doi.org/10.1016/j.soilbio.2025.109831.

Hudson, N., Ayoko, G.A., 2008. Odour sampling. 2. Comparison of physical and aerodynamic characteristics of sampling devices: a review. Bioresour. Technol. 99, 3993–4007. https://doi.org/10.1016/j.biortech.2007.03.043.

Ibrom, A., Dellwik, E., Flyvbjerg, H., Jensen, N.O., Pilegaard, K., 2007. Strong low-pass filtering effects on water vapour flux measurements with closed-path eddy correlation systems. Agric. For. Meteorol. https://doi.org/10.1016/j.agrformet.2007.07.007.

Kljun, N., Calanca, P., Rotach, M.W., Schmid, H.P., 2015. A simple two-dimensional parameterisation for Flux Footprint Prediction (FFP). Geosci. Model Dev. 8, 3695–3713. https://doi.org/10.5194/gmd-8-3695-2015.

Lallo, M., Aalto, T., Hatakka, J., Laurila, T., 2009. Hydrogen soil deposition at an urban site in Finland. Atmos. Chem. Phys. 9, 8559–8571. https://doi.org/10.5194/acp-9-8559-2009.

Mauder, M., Foken, T., 2004. Documentation and Instruction Manual of the Eddy Covariance Software Package TK2. Univ Bayreuth, Abt Mikrometeorol, pp. 26–42. https://epub.uni-bayreuth.de/884/1/ARBERG026.pdf. (Accessed 24 November 2025).

Meredith, L.K., Commane, R., Keenan, T.F., Klosterman, S.T., Munger, J.W., Templer, P. H., Tang, J., Wofsy, S.C., Prinn, R.G., 2016. Ecosystem fluxes of hydrogen in a mid-latitude forest driven by soil microorganisms and plants. Glob. Change Biol. 23, 906–919. https://doi.org/10.1111/gcb.13463.

Meredith, L.K., Commane, R., Munger, J.W., Dunn, A., Tang, J., Wofsy, S.C., Prinn, R.G., 2014. Ecosystem fluxes of hydrogen: a comparison of flux-gradient methods. Atmos. Meas. Tech. 7, 2787–2805. https://doi.org/10.5194/amt-7-2787-2014.

Momeni, A., Albertson, J.D., Herndon, S., Daube, C., Nelson, D., Roscioli, J.R., Shorter, J., Lunny, E., Wehr, R., Gadikota, G., Cui, Y., Sun, T., 2025. Quantification of hydrogen emission rates using downwind plume characterization techniques. Environ. Sci. Technol. 59, 6016–6024. https://doi.org/10.1021/acs.est.4c13616.

Moncrieff, J.B., Massheder, J.M., de Bruin, H., Elbers, J., Friborg, T., Heusinkveld, B., Kabat, P., Scott, S., Soegaard, H., Verhoef, A., 1997. A system to measure surface fluxes of momentum, sensible heat, water vapour and carbon dioxide. J. Hydrol. https://doi.org/10.1016/s0022-1694(96)03194-0.

Moravek, A., Foken, T., Trebs, I., 2014. Application of a GC-ECD for measurements of biosphere–atmosphere exchange fluxes of peroxyacetyl nitrate using the relaxed eddy accumulation and gradient method. Atmos. Meas. Tech. 7, 2097–2119. https://doi.org/10.5194/amt-7-2097-2014.

Morfopoulos, C., Foster, P.N., Friedlingstein, P., Bousquet, P., Prentice, I.C., 2012. A global model for the uptake of atmospheric hydrogen by soils. Glob. Biogeochem. Cycles 26. https://doi.org/10.1029/2011gb004248.

Nagai, M., Kakiuchi, H., Masuda, T., 2024. Measurements of hydrogen deposition velocities by farmland soil using $D_2$ gas. Radiat. Protect. Dosim. 200, 1763–1766. https://doi.org/10.1093/rpd/ncae055.

Novelli, P.C., Lang, P.M., Masarie, K.A., Hurst, D.F., Myers, R., Elkins, J.W., 1999. Molecular hydrogen in the troposphere: global distribution and budget. J. Geophys. Res. 104, 30427–30444. https://doi.org/10.1029/1999jd900788.

Ocko, I.B., Hamburg, S.P., 2022. Climate consequences of hydrogen emissions. Atmos. Chem. Phys. 22, 9349–9368. https://doi.org/10.5194/acp-22-9349-2022.

Ouyang, Z., Jackson, R.B., Saunois, M., Canadell, J.G., Zhao, Y., Morfopoulos, C., Krummel, P.B., Patra, P.K., Peters, G.P., Dennison, F., Gasser, T., Archibald, A.T., Arora, V., Baudoin, G., Chandra, N., Ciais, P., Davis, S.J., Feron, S., Guo, F., Hauglustaine, D., Jones, C.D., Jones, M.W., Kato, E., Kennedy, D., Knauer, J., Lienert, S., Lombardozzi, D., Melton, J.R., Nabel, J.E.M.S., O'Sullivan, M., Pétron, G., Poulter, B., Rogelj, J., Sandoval Calle, D., Smith, P., Suntharalingam, P., Tian, H., Wang, C., Wiltshire, A., 2025. The global hydrogen budget. Nature 648, 616–624. https://doi.org/10.1038/s41586-025-09806-1.

Panofsky, H.A., 1963. Determination of stress from wind and temperature measurements. Q. J. R. Meteorol. Soc. 89, 85–94. https://doi.org/10.1002/qj.49708937906.

Paulot, F., Pétron, G., Crotwell, A.M., Bertagni, M.B., 2024. Reanalysis of NOAA $H_2$ observations: implications for the $H_2$ budget. Atmos. Chem. Phys. 24, 4217–4229. https://doi.org/10.5194/acp-24-4217-2024.

Paulson, C.A., 1970. The mathematical representation of wind speed and temperature profiles in the unstable atmospheric surface layer. J. Appl. Meteorol. 9 (2), 857–861. https://doi.org/10.1175/1520-0450(1970)009<0857:tmrows>2.0.co.

Pétron, G., Crotwell, A.M., Mund, J., Crotwell, M., Mefford, T., Thoning, K., Hall, B., Kitzis, D., Madronich, M., Moglia, E., Neff, D., Wolter, S., Jordan, A., Krummel, P., Langenfelds, R., Patterson, J., 2024. Atmospheric $H_2$ observations from the NOAA cooperative global air sampling network. Atmos. Meas. Tech. 17, 4803–4823. https://doi.org/10.5194/amt-17-4803-2024.

R Core Team, 2025. R: a Language and Environment for Statistical Computing. R Foundation for Statistical Computing, Vienna, Austria. https://www.R-project.org/.

Rahn, T., Eiler, J.M., Kitchen, N., Fessenden, J.E., Randerson, J.T., 2002. Concentration and δD of molecular hydrogen in boreal forests: ecosystem-scale systematics of atmospheric $H_2$. Geophys. Res. Lett. 29. https://doi.org/10.1029/2002gl015118.

Reji, L., Bertagni, M.B., Paulot, F., Qin, Q., Zhang, X., 2025. Moisture controls on hydrogen oxidizing bacteria: implications for the. Global Soil Hydrogen Sink. https://doi.org/10.1101/2025.04.18.649571.

Rezaei, S., Hormaza Mejia, A., Wu, Y., Reed, J., Brouwer, J., 2025. Global warming impacts of the transition from fossil fuel conversion and infrastructure to hydrogen. Appl. Energy 397, 126363. https://doi.org/10.1016/j.apenergy.2025.126363.

Rhee, T.S., Brenninkmeijer, C.A.M., Röckmann, T., 2006. The overwhelming role of soils in the global atmospheric hydrogen cycle. Atmos. Chem. Phys. 6, 1611–1625. https://doi.org/10.5194/acp-6-1611-2006.

Sand, M., Skeie, R.B., Sandstad, M., Krishnan, S., Myhre, G., Bryant, H., Derwent, R., Hauglustaine, D., Paulot, F., Prather, M., Stevenson, D., 2023. A multi-model assessment of the Global Warming Potential of hydrogen. Commun. Earth Environ. 4. https://doi.org/10.1038/s43247-023-00857-8.

Seinfeld, J.H., Pandis, S.N., 2006. Atmospheric Chemistry and Physics: from Air Pollution to Climate Change, second ed. John Wiley & Sons (Wiley-Interscience, Hoboken, NJ.

Simmonds, P.G., Derwent, R.G., Manning, A.J., Grant, A., O'doherty, S., Spain, T.G., 2011. Estimation of hydrogen deposition velocities from 1995–2008 at Mace Head, Ireland using a simple box model and concurrent ozone depositions. Tellus B 63, 40. https://doi.org/10.1111/j.1600-0889.2010.00518.x.

Smith-Downey, N.V., Randerson, J.T., Eiler, J.M., 2008. Molecular hydrogen uptake by soils in forest, desert, and marsh ecosystems in California. J. Geophys. Res. 113. https://doi.org/10.1029/2008jg000701.

Warwick, N.J., Archibald, A.T., Griffiths, P.T., Keeble, J., O'Connor, F.M., Pyle, J.A., Shine, K.P., 2023. Atmospheric composition and climate impacts of a future hydrogen economy. Atmos. Chem. Phys. 23, 13451–13467. https://doi.org/10.5194/acp-23-13451-2023.

Webb, E.K., 1970. Profile relationships: the log-linear range, and extension to strong stability. Q. J. R. Meteorol. Soc. 96, 67–90. https://doi.org/10.1002/qj.49709640708.

Wood, S.N., 2017. Generalized Additive Models. Chapman and Hall/CRC. https://doi.org/10.1201/9781315370279.

Xu, L., Furtaw, M.D., Madsen, R.A., Garcia, R.L., Anderson, D.J., McDermitt, D.K., 2006. On maintaining pressure equilibrium between a soil $CO_2$ flux chamber and the ambient air. J. Geophys. Res. 111. https://doi.org/10.1029/2005jd006435.

Yonemura, S., Kawashima, S., Tsuruta, H., 2000. Carbon monoxide, hydrogen, and methane uptake by soils in a temperate arable field and a forest. J. Geophys. Res. 105, 14347–14362. https://doi.org/10.1029/1999jd901156.

Yver, C., Schmidt, M., Bousquet, P., Zahorowski, W., Ramonet, M., 2009. Estimation of the molecular hydrogen soil uptake and traffic emissions at a suburban site near Paris through hydrogen, carbon monoxide, and radon-222 semicontinuous measurements. J. Geophys. Res. 114. https://doi.org/10.1029/2009jd012122.